Preparation and characterization of nanocellulose-reinforced water-soluble cellulose acetate films

Reactive and Functional Polymers 205 (2024) 106083

Contents lists available at ScienceDirect

Reactive and Functional Polymers

journal homepage: www.elsevier.com/locate/react

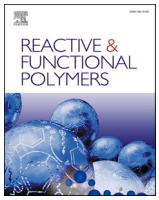

Preparation and characterization of nanocellulose-reinforced water-soluble cellulose acetate films

Hongrun Chen [a,b], Gaoyuan Hou [a], Korawit Chitbanyong [a], Miyuki Takeuchi [a], Izumi Shibata [a], Akira Isogai [a,*]

[a] Department of Biomaterial Science, the University of Tokyo, Japan
[b] Chalmers University of Technology, Sweden

ARTICLE INFO

Keywords:
Cellulose acetate
Composite film
TEMPO
Tensile property
Water-base system

ABSTRACT

A water-soluble cellulose acetate (CA) with a degree of acetyl substitution of 0.9 was dissolved in water and mixed with aqueous dispersions of reinforcing cellulose nanofibers (CNFs) at various mass ratios. CA/CNF composite films with CNF contents of 0 %–16 % were prepared by casting and drying the mixtures to improve the fundamental properties of the films. Aqueous dispersions of TEMPO-CNFs containing sodium carboxylate and protonated carboxy groups were separately prepared and used to produce CA composite films (TEMPO = 2,2,6,6-tetramethylpiperidine-1-oxyl radical). Highly transparent CA/TEMPO-CNF films with tensile strengths and Young's moduli more than twofold those of the 100 % CA film were obtained at a TEMPO-CNF content of 16 %. Transmission electron microscopy images of the film cross-sections showed that the TEMPO-CNFs were almost homogeneously and individually distributed in the CA/TEMPO-CNF-COOH composite films. The thermal expansion patterns of the 100 % CA films were characteristically wavy between 30 and 100 °C, and the thermal expansion ratios decreased as the TEMPO-CNF contents of the films increased. The obtained results indicate that CA/CNF mixtures can be used as water-based coatings and paints with favorable properties.

1. Introduction

Commercial cellulose acetates include cellulose diacetate (CDA) and cellulose triacetate (CTA), with degrees of substitution (DSs) of ~3 and ~ 2.4, respectively, and are the most abundantly produced cellulose derivatives. CDA and CTA are used as fibers and films, primarily for clothes/filters and liquid crystalline displays, respectively [1,2]. These cellulose acetates (CAs) are soluble in organic solvents, and can be formed into fibers or films by wet-spinning or casting from organic solutions, and simultaneous or subsequent removal of the organic solvent [2]. CA fibers and films have unique and characteristic properties that are absent from petroleum-based synthetic fibers or films [2,3]. However, the use of organic solvents is a major concern from an environmental perspective.

Cellulose ethers are water-soluble cellulose derivatives that are produced on an industrial scale; they are used, for example, as thickeners for commodity products, in foods, and in coating films in the paper industry [4]. The preparation of water-soluble CAs and their properties have been reported in the literature [5–8]. The control of DS values by non-aqueous organic cellulose solvent systems or ionic liquids as homogeneous acetylation media has been proposed [5,6], but has not been widely adopted by industry. The partial deacetylation from homogeneous CTA/acetic anhydride/acetic anhydride solutions with catalytic amounts of sulfuric acid, obtained in the CTA production process, to CAs with DSs of ~1.0 via CDA is a promising industrial process [7–10]. Furthermore, the biodegradability of water-soluble CAs is an attractive and environmentally friendly attribute [11–13].

Water-soluble CAs have been reported for pharmaceutical applications [14]. However, they have low DPs and consequently do not have the mechanical properties required for coating and painting materials [5–8]. If the mechanical properties of CAs can be improved, their applications may be quantitatively and qualitatively expanded, because water-based systems that comprise CAs are favorable in terms of environmental issues.

Cellulose nanofibers (CNFs) are prepared from native cellulose fibers by chemical or enzymatic pretreatments and subsequent mechanical fibrillation in water to obtain aqueous dispersions [15]. Commercially available TEMPO-oxidized CNFs (TEMPO = tetramethylpiperidine-1-

* Corresponding author.
E-mail address: akira-isogai@g.ecc.u-tokyo.ac.jp (A. Isogai).

https://doi.org/10.1016/j.reactfunctpolym.2024.106083
Received 29 July 2024; Received in revised form 23 October 2024; Accepted 27 October 2024
Available online 29 October 2024

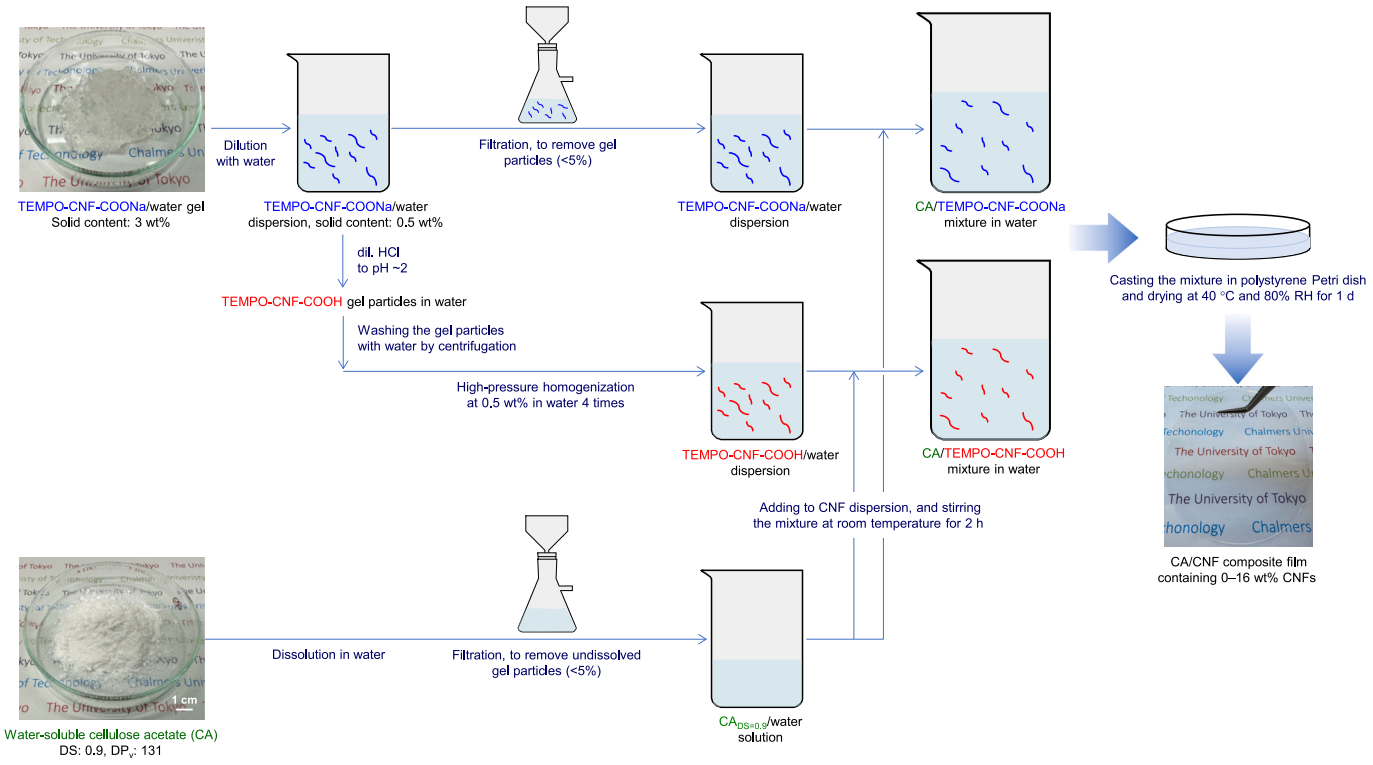

Fig. 1. Preparation of $CA_{DS=0.9}$/TEMPO-CNF composite films.

oxyl radical) with homogeneous widths of ~3 nm and average lengths of >400 nm have been produced on an industrial scale. TEMPO-CNF films have high optical transparencies, tensile strengths, and Young's moduli [15–17]. They also have extremely low coefficients of thermal expansion, owing to their cellulose I crystal structures, as well as nano-sized morphologies [16,17], and controllable biodegradability [18]. If mechanically weak water-soluble CA films are reinforced by TEMPO-CNFs using water systems as mixing media, and subsequent casting and drying, their applications are quantitatively and qualitatively expanded.

Cast and dried composite films containing TEMPO-CNFs have been prepared by mixing aqueous TEMPO-CNF dispersions and aqueous solutions of cellulose ethers [4], polyvinyl alcohol [19], polyacrylamide [20], and polyethylene oxide [21] as matrix polymers. The reinforcing effects of TEMPO-CNFs on the properties of composite films vary, depending on the water-soluble matrix polymers used. CA/TEMPO-CNF composite films may have potential as biodegradable cellulose-based polymers with superior properties for coatings and paints.

In the present work, we separately dissolved a water-soluble CA in water, and dispersed aqueous TEMPO-CNFs with sodium carboxylate and protonated carboxy groups (TEMPO-CNF-COONa and TEMPO-CNF-COOH, respectively). We prepared CA composite films with TEMPO-CNF contents of 0 %–16 % by mixing aqueous CA solutions and aqueous TEMPO-CNF dispersions at various mass ratios, and casing and drying the mixtures. The optical, mechanical, and thermal properties of the CA/TEMPO-CNF composite films were investigated in terms of the TEMPO-CNF contents of the films, and the structures of their carboxy groups. The results showed that the CA/TEMPO-CNF composite films had mechanical and thermal properties that were superior to those of the neat 100 % CA film. The water-soluble CA is categorized as a functional polymer, and the counterions of carboxy groups in TEMPO-CNFs can be controlled by simple ion-exchange in water. The interactions between the CA molecules and TEMPO-CNFs in the composite films may be different, depending on the counterions of TEMPO-CNFs. Thus, the water-soluble CA and TEMPO-CNFs used for preparation of composite films in this study are regarded as functional and reactive polymers.

2. Materials and methods

2.1. Materials

A commercial 3 wt% TEMPO-CNF-COONa/water gel prepared from softwood bleached kraft pulp was provided by Nippon Paper Industries Co., Ltd., Japan. The carboxy content of the CNFs was 1.5 mmol/g. A commercial water-soluble CA produced by a Japanese company was used [22,23]. The degree of substitution and viscosity average degree of polymerization of the CA were 0.9 of 131, respectively, according to the catalog data. Deionized water was used in all experiments.

2.2. Preparation of composite films

The 3 wt% TEMPO-CNF-COONa/water gel was diluted with water and stirred to produce a viscous 0.5 wt% homogeneous dispersion. The $CA_{DS=0.9}$ powder (CA with a DS of 0.9) was dissolved in water to produce a 3 wt% solution. The TEMPO-CNF dispersion or the CA solution was filtered on a 20 μm membrane filter under reduced pressure to remove small gel particles or insoluble fractions, which constituted less than 5 wt% of the dry mass of the original CNFs or CA. A TEMPO-CNF-COOH/water dispersion was prepared according to the procedure reported previously [24], with slight modification. Briefly, a dilute HCl solution was slowly added to the 0.5 wt% TEMPO-CNF-COONa/water homogeneous dispersion to maintain the pH at ~2, and the mixture was stirred for 30 min. The viscosity of the mixture increased, and gel particles were formed in the mixture. The gel particles were washed with water by centrifugation for 10 min × 4 times to remove excess HCl. The particles/water suspension was subjected to high-pressure homogenization (NanoVater NVC-ES008A-D10, Yoshida Kikai, Co., Japan) four times to prepare a transparent, homogeneous, and viscous TEMPO-CNF-COOH/water dispersion.

$CA_{DS=0.9}$/TEMPO-CNF composite films were prepared by casting and

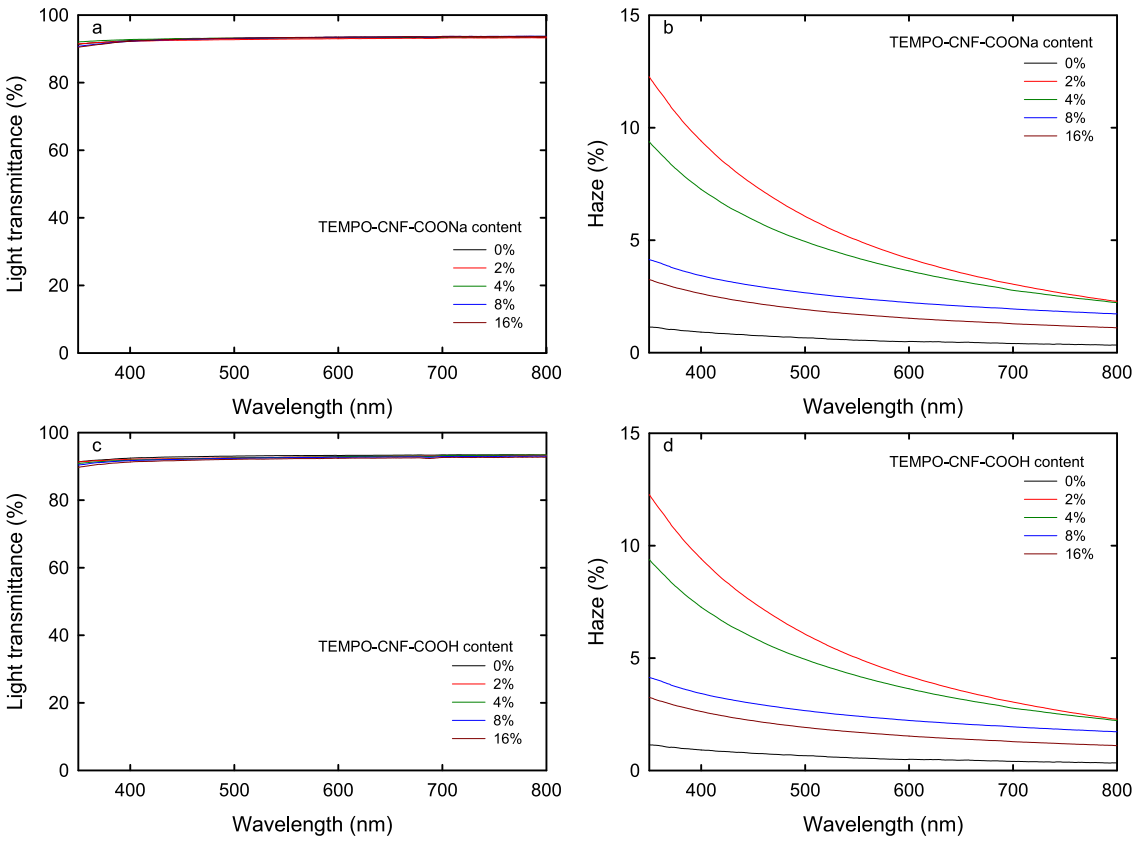

Fig. 2. (a,c) Light transmittance and (b,d) haze spectra of (a,b) $CA_{DS=0.9}$/TEMPO-CNF-COONa and (c,d) $CA_{DS=0.9}$/TEMPO-CNF-COOH composite films.

drying. A 3.0 wt% $CA_{DS=0.9}$ solution and either a 0.5 wt% TEMPO-CNF-COONa or TEMPO-CNF-COOH dispersion were mixed, and the mixture was stirred at ~23 °C for 2 h. Each mixture was degassed in a Thinky AR-100 planetary centrifugal mixer at 2200 rpm and 23 °C for 3 min. The degassing process was repeated twice. The $CA_{DS=0.9}$/TEMPO-CNF mixtures were poured into polystyrene petri dishes and dried in an oven at 40 °C and 80 % relative humidity (RH) for more than 1 day. The dried films were separated from the petri dishes and stored at 23 °C and 50 % RH for more than 1 day (Fig. 1). The TEMPO-CNF contents of the composite films were 0 %, 2 %, 4 %, 8 %, and 16 % by dry mass.

2.3. Analyses

Solution and solid-state carbon 13 nuclear magnetic resonance (^{13}C NMR) spectra of CA were obtained using a JNM-ECA II 500 spectrometer (JEOL, Tokyo, Japan). Each CA sample was dissolved in deuterium oxide (D_2O) for solution-state NMR analysis. The solid-state ^{13}C NMR spectra of CA were obtained according to a previously reported method [25]. The moisture content of each film at 23 °C and 50 % RH was measured by drying the film at 105 °C for 3 h. The Fourier-transform infrared (FT-IR) spectrum of each film was obtained using an FT/IR-6100 spectrometer (JASCO, Tokyo, Japan) in transmission mode at a 4 cm^{-1} resolution. A V-670 UV–vis spectrophotometer (JASCO, Tokyo, Japan) was used to measure the light transmittance and haze values of each film. The light transmittances were normalized to a thickness of 40 μm using the Beer–Lambert law [26]. The haze value of each film was calculated from its total and diffusive light transmittances according to American Society for Testing and Materials standard D1003 [27]. The surface of each film was investigated using an optical microscope (SZX2-ILLTS, Evident Co., Japan). The tensile properties of each film were determined using an EZ-SX tensile tester (Shimadzu, Tokyo, Japan) with a 500 N load cell. The films were cut into 2 × 30 mm strips, and the tests were conducted on span lengths of 10 mm at speeds of 0.5 mm/min. At least five strips were tested for each sample.

The X-ray diffraction (XRD) pattern of each film was obtained using a MiniFlex 600 system (Rigaku, Tokyo, Japan) at 40 kV and 15 mA. The particle sizes of the two CNF dispersions at ~0.0125 % solid contents were measured using a laser particle size analyzer (Litesizer 500, Anton Paar, Austria). Each film was swollen in 50 vol% ethanol/water to increase its thickness [4]. Each swollen sample was soaked in a series of ethanol/water mixtures with ethanol concentrations that gradually increased up to 100 %. This enabled solvent exchange from water to ethanol in the film, maintaining its original form. Each film sample was then fixed in an epoxy resin. Ultrathin sections of the film were then prepared using an Ultramicrotome (Ultracut-UTC, Leica, Germany). The ultrathin sections were stained with 4 wt% uranyl acetate and Reynold's lead citrate solutions. Transmission electron microscopy (TEM) images of the film sections were obtained using a JEM-1400 Plus system operated at 100 kV. Each film sample was dried at 102 °C in a nitrogen stream for 30 min, and its thermal expansion was measured using a TMA60 system (Shimadzu, Tokyo, Japan) [16]. The measurements were obtained at 30–100 °C at a heating rate of 5 °C/min with an applied force of 0.03 N.

3. Results and discussion

3.1. Structural characterization of the $CA_{DS=0.9}$ and TEMPO-CNFs

The commercial CA sample was analyzed by solid- and solution-state ^{13}C NMR spectroscopy (Fig. S1 in the Supplementary Data). The signal area ratios of the methyl carbons of the acetyl groups/C1 in the solid- and solution-state ^{13}C NMR spectrum were 0.91 and 0.87, respectively, and were almost the same as the DS value (0.9) reported in the catalog data. The C6/C1 signal area ratio of cellulose in the solid-state ^{13}C NMR spectra is always lower than 0.8 because two protons are linked to the C6 carbon [28]. The signal area ratios of C2,3,4,5/C1 in the solid- and

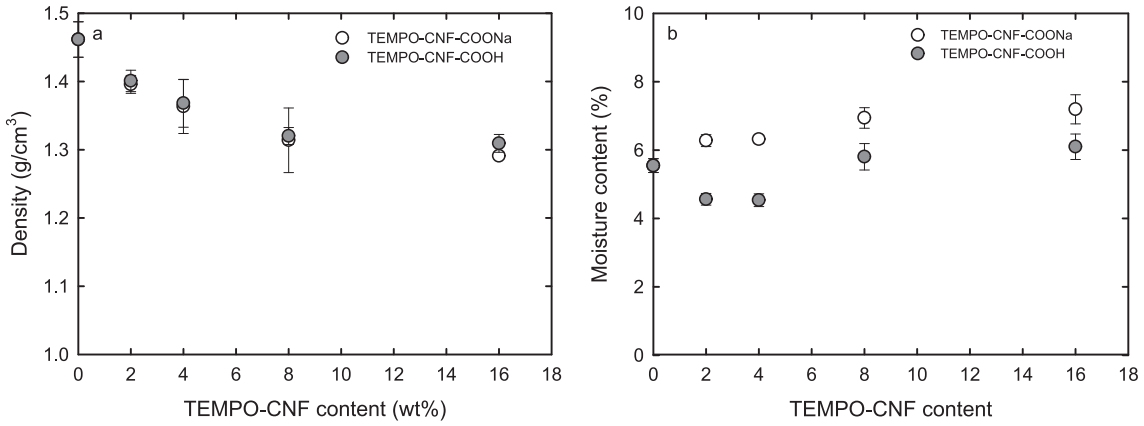

Fig. 3. (a) Density and (b) moisture content of the $CA_{DS=0.9}$/TEMPO-CNF composite films.

solution-state ^{13}C NMR spectra were 4.01 and 3.86, respectively, and were roughly similar to the quantitative value. The C═O signal areas of the acetyl groups linked to the hydroxy groups of C2, C3, and C6 in the solution-state ^{13}C NMR spectra indicated the distributions of the acetyl groups between the three hydroxy groups of the glycosyl units in the cellulose. Although the NMR spectrum was not obtained in the quantitative mode, and the corresponding peaks overlapped each other (Fig. S1a, left below inset), the distribution of acetyl groups followed the approximate order C6 > C3 > C2, which was slightly different from the orders reported previously [29,30].

The FT-IR spectra of the TEMPO-CNF-COONa and TEMPO-CNF-COOH films are shown in Fig. S2 in the Supplementary Data. The TEMPO-CNF-COONa film had a C═O stretching absorption peak at 1600 cm^{-1} that was attributable to sodium carboxy groups, but no C═O absorption peak that was attributable to protonated carboxy groups. In contrast, the TEMPO-CNF-COOH film had a C═O stretching absorption peak at 1720 cm^{-1} that was attributable to protonated carboxy groups [24]. Therefore, the counterion exchange from TEMPO-CNF-COONa to TEMPO-CNF-COOH was successfully achieved by the procedure used in this study. The average particle sizes of the TEMPO-CNF-COONa and TEMPO-CNF-COOH dispersed in water at ~0.125 % solid contents were 512 nm and 304 nm, respectively (Fig. S3 in the Supplementary Data). Thus, the average particle size of the TEMPO-CNF-COOH sample decreased from that of the TEMPO-CNF-COONa probably by additional high-pressure homogenization four times in water. Shortening of the fibril length of the TEMPO-CNF-COONa and/or fibrillation of the TEMPO-CNF-COONa aggregates may have partly occurred during the homogenization treatment.

3.2. *Preparation of the $CA_{DS=0.9}$/TEMPO-CNF composite films and their fundamental properties*

The CA/TEMPO-CNF composite films were prepared according to the scheme shown in Fig. 1. The aqueous CA/TEMPO-CNF mixtures were degassed and dried at 80 % RH to provide smooth and transparent films in 1 day. The dried CA/TEMPO-CNF composite films were smoothly removed from the petri dishes without any problems such as tearing or breaking, whereas the 100 % CA films were difficult to be smoothly removed from the petri dishes.

All the composite films were visibly transparent (Fig. S4 in the Supplementary Data). The light transmittances and haze spectra of the films are shown in Fig. 2. All the films exhibited high light transmittances of ~93 % at 600 nm, indicating that the TEMPO-CNFs were homogeneously and individually nano-dispersed in the CA matrix without forming aggregates, irrespective of the TEMPO-CNF content.

The haze spectra of the composite films were surprising. All the haze values were sufficiently low as transparent films, but the 2 % TEMPO-CNF-containing composite films had the highest haze values, which decreased with increasing TEMPO-CNF content in both composite systems. The 16 % TEMPO-CNF-containing composite films had the lowest

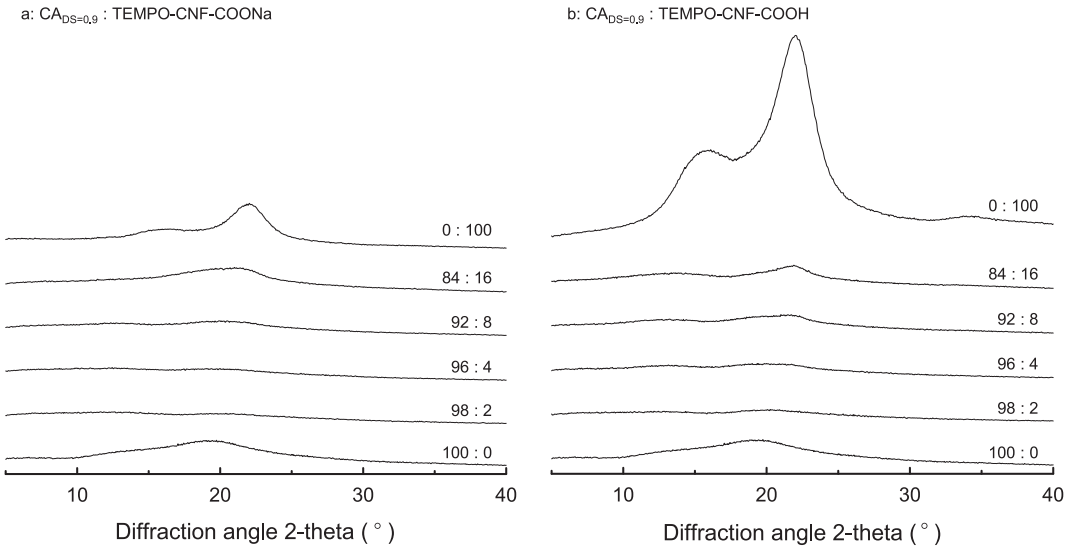

Fig. 4. X-ray diffraction patterns of (a) $CA_{DS=0.9}$/TEMPO-CNF-COONa and (b) $CA_{DS=0.9}$/TEMPO-CNF-COOH composite films.

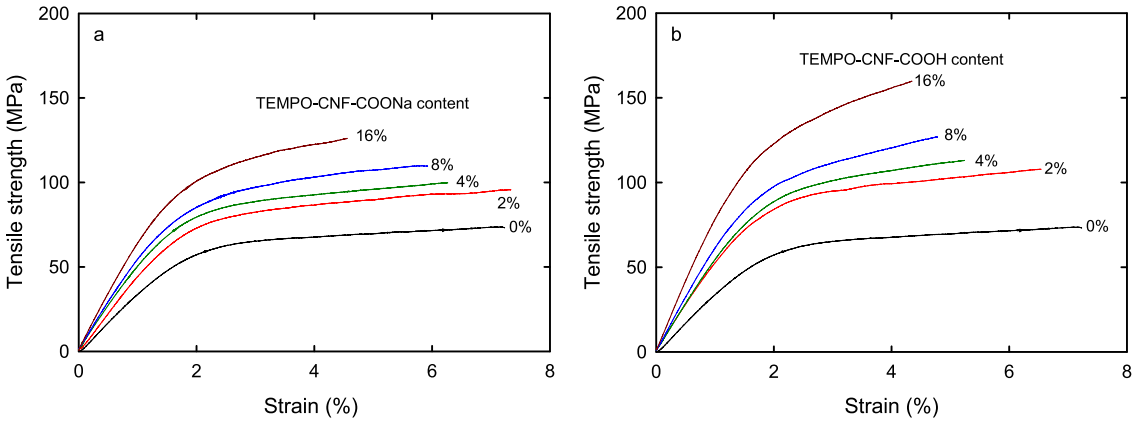

Fig. 5. Representative stress–strain curves of (a) $CA_{DS=0.9}$/TEMPO-CNF-COONa and (b) TEMPO-CNF-COOH composite films.

haze values, which were slightly higher than that of the 100 % CA film. Fig. S5 in the Supplementary Data shows microphotographs of the surfaces of the composite films prepared with 2 % and 16 % TEMPO-CNF-COONa. The 16 % TEMPO-CNF-containing film surface was smoother at the micrometer level than that of the 2 % TEMPO-CNF-containing film. This result indicated that rougher film surfaces were formed as the TEMPO-CNF content was decreased from 16 % to 2 %. Similar results about the influence of surface roughness on the haze values were reported for nanocellulose film samples [31–33]. Probably the water-removal speeds differed between the $CA_{DS=0.9}$/water solution and the TEMPO-CNF/water dispersion at 40 °C and 80 % RH, resulting in the formation of composite films with rougher surfaces. However, this hypothesis should be investigated further to obtain evidence.

The densities and moisture contents of the films are presented in Fig. 3. The film density decreased from 1.5 g/cm^3 for the 100 % CA film to 1.3 g/cm^3 with an increase in TEMPO-CNF content up to 16 % in similar manners in the two systems. These results are similar to those of film densities of TEMPO-CNF-containing polyacrylamide or polyvinyl alcohol composites [20]. The presence of crystalline TEMPO-CNFs in the CA matrix polymer may have caused a decrease in the amount of some ordered structures (corresponding to the high density) in the CA matrix polymer. Another possibility to explain the obtained results is that the presence of TEMPO-CNFs in the composite films may have increased pore volumes as in the cases of TEMPO-CNF-containing polyacrylamide and polyvinyl alcohol composite films [20]. However, the reasons for the results in Fig. 3a are unknown at present. Because there were no clear differences in the film densities at the same TEMPO-CNF contents between the sodium carboxylate and protonated carboxy groups in the films, the CA/CNF interface structures or the densities of the CA/CNF interface layers might be similar in the two systems.

As expected, the moisture content increased as the hydrophilic TEMPO-CNF-COONa content increased in the composite films. When TEMPO-CNF-COOH was added, the moisture contents of the composite films with CNF contents of 2 % and 4 % were lower than that of the 100 % CA film. The moisture contents of the 8 % and 16 % TEMPO-CNF-COOH-containing CA composite films were slightly higher than that of

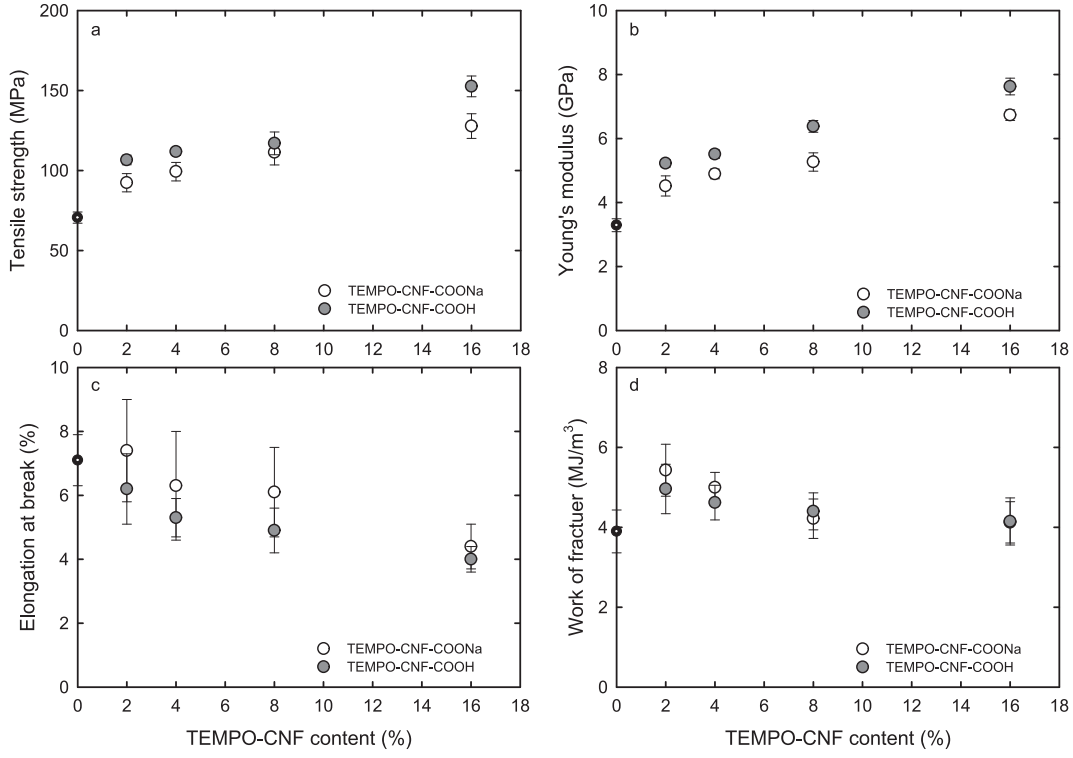

Fig. 6. Tensile properties of $CA_{DS=0.9}$/TEMPO-CNF composite films: (a) tensile strength, (b) Young's modulus, (c) elongation at break, and (d) work of fracture.

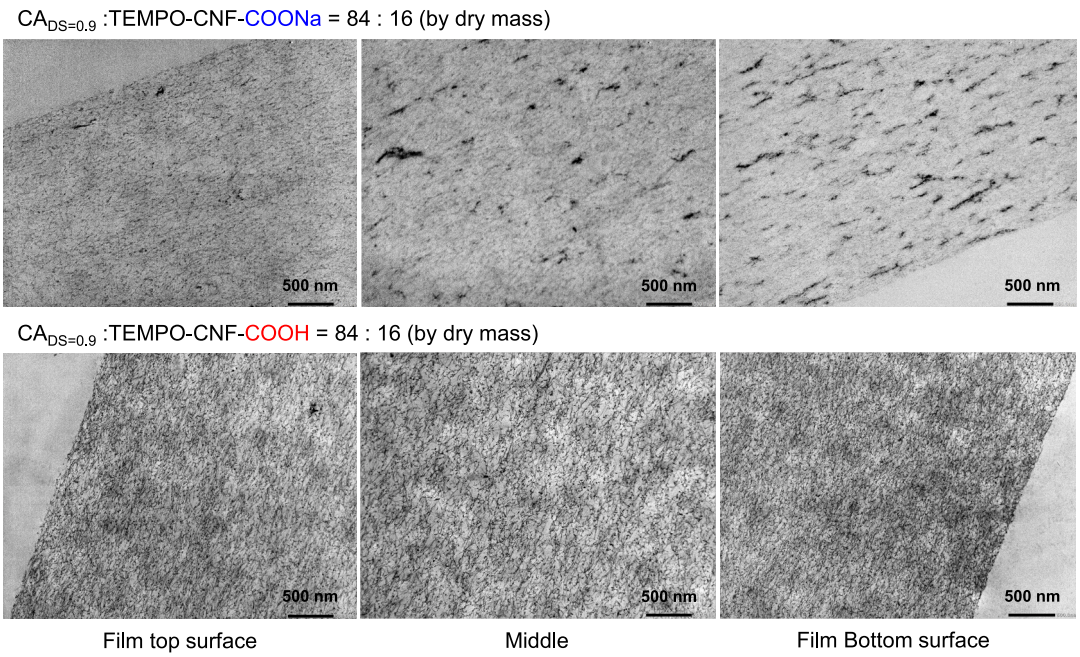

Fig. 7. TEM images of cross-sections (top surface, middle, and bottom surface) of the CA$_{DS=0.9}$/TEMPO-CNF-COONa and CA$_{DS=0.9}$/TEMPO-CNF-COOH composite films.

the 100 % CA film. These moisture contents of the TEMPO-CNF-COOH-containing CA composite films may be explained in terms of the formation of less hydrophilic hydrogen bonds between the hydroxy groups of the CA molecules and the protonated carboxy groups of TEMPO-CNF-COOH.

The XRD patterns of the composite films are shown in Fig. 4. The broad peak at diffraction angles of 10–25° revealed the disordered structures in CA. The XRD patterns of the CA/TEMPO-CNF composite films became flatter, indicating that some of the ordered structures of the 100 % CA film became less ordered when the TEMPO-CNFs were added. Although the 100 % TEMPO-CNF-COONa film and the 100 % TEMPO-CNF-COOH film exhibited different intensities of the cellulose I crystal structure [16], their Segal's crystallinities were the same (69 %), and their crystal widths, which were calculated from the full widths of the (200) peaks, were also the same (3.1 nm). Thus, the presence of Na counterions in the 100 % TEMPO-CNF-COONa film caused a decrease in XRD intensity, but the crystallinity and the crystal width of cellulose I were the same in the 100 % TEMPO-CNF-COONa film as in the 100 % TEMPO-CNF-COOH film.

3.3. *Tensile properties of the CA$_{DS=0.9}$/TEMPO-CNF composite films*

Typical stress–strain curves of the CA/TEMPO-CNF composite films are shown in Fig. 5. The tensile strengths and Young's moduli of the films increased as the TEMPO-CNF contents increased because TEMPO-CNFs are crystalline nanofibers with high elastic moduli of ~140 GPa [16,34]. However, the elongation at break values decreased following the addition of CNFs. In particular, the addition of TEMPO-CNF-COOH to CA resulted in higher tensile strengths and Young's moduli, indicating that the formation of hydrogen bonds between the hydroxy groups of CA$_{DS=0.9}$ and the protonated carboxy groups of the TEMPO-CNFs at the interface layers improved these properties.

The tensile properties of the composite films are plotted against their TEMPO-CNF contents in Fig. 6. The tensile strengths and Young's moduli clearly increased as the TEMPO-CNF contents increased. In particular, the tensile strength and Young's modulus of the 16 % TEMPO-CNF-containing CA composite film increased by more than twofold compared with those of the 100 % CA film. The addition of TEMPO-CNF-COOH resulted in higher tensile strengths and Young's moduli than the addition of TEMPO-CNF-COONa at the same TEMPO-CNF content. The results shown in Fig. 6a, b were probably the result of the protonated carboxy groups in the TEMPO-CNFs forming hydrogen bonds with the hydroxy groups of the CA molecules, as discussed in the previous paragraph based on the results shown in Fig. 5.

In contrast, the elongation at break values decreased as the TEMPO-CNF contents of the composite films increased (Fig. 6c). The work of fracture of the composite films was highest at a TEMPO-CNF content of 2 %. The tensile strength, Young's modulus, and elongation at break values of the composite films are plotted against the densities or moisture contents of the composite films in Fig. S6 in the Supplementary Data. The Young's moduli of composite films are often governed by the film densities, and the moisture contents of the films influence their elongations at break or works of fracturs [17,21]. Although the film density decreased with increasing TEMPO-CNF content for both the TEMPO-CNF-COONa- and TEMPO-CNF-COOH-containing CA composite films (Figs. 3a, S6e), their Young's moduli increased with the CNF content, which is unexpected but similar to the results of TEMPO-CNF-containing polyvinyl alcohol and polyacrylamide composite films [20]. Thus, the presence of high-modulus TEMPO-CNFs in the CA composite film may have overcome the influence of the decreased film density on the Young's modulus of the composite film. The moisture contents of the composite films were roughly constant against their TEMPO-CNF contents (Fig. 3b). Thus, the elongation at break decreased with the CNF content, which was primarily governed by the increased Young's modulus. Consequently, the addition of crystalline and high-modulus TEMPO-CNFs to the amorphous CA base polymer influenced the resultant tensile properties of the composite films.

TEM images of the cross-sections of the 16 % TEMPO-CNF-containing CA composite films are shown in Fig. 7. The top surface layer of the TEMPO-CNF-COONa-containing film consisted of almost homogeneously distributed TEMPO-CNFs, whereas the middle and bottom surface layers consisted of partly aggregated TEMPO-CNFs. In contrast, in the TEMPO-CNF-COOH-containing film, the TEMPO-CNFs maintained their original nanofiber structures and morphologies, and were homogeneously nano-dispersed without forming any aggregates in the three layers of the film.

The TEMPO-CNF-COOH elements were homogeneously and individually nano-distributed in the CA matrices of the composite films. This

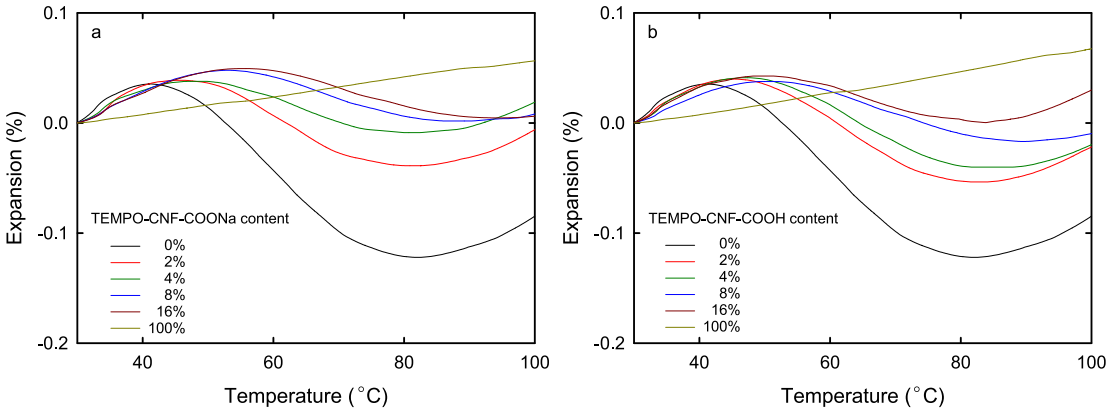

Fig. 8. Coefficient of thermal expansion values of (a) $CA_{DS=0.9}$/TEMPO-CNF-COONa and (b) $CA_{DS=0.9}$/TEMPO-CNF-COOH composite films.

may have been the cause of the higher tensile strengths, Young's moduli, and work of fracture values of those films compared with those of the CA/TEMPO-CNF-COONa composite films at the same TEMPO-CNF contents, as shown in Fig. 5 and Fig. 6. When TEMPO-CNFs form aggregates in CA matrices such as TEMPO-CNF-COONa-containing composite films, the relative aspect ratios of the CNFs decrease, resulting in composite films with lower tensile moduli [4,35].

3.4. Thermal properties of the $CA_{DS=0.9}$/TEMPO-CNF composite films

The thermal expansion behaviors of the films were investigated by thermomechanical analysis, and the results are shown in Fig. 8. The thermal expansion values of the 100 % TEMPO-CNF-COONa and TEMPO-CNF-COOH films increased linearly with temperature [16], and their coefficients of thermal expansion (CTE) were 8.3 and 9.9 ppm/K, respectively. The CTE values of these TEMPO-CNF films were quite low and close to the CTE of glass [16] owing to the crystalline structures of the TEMPO-CNFs. The 100 % $CA_{DS=0.9}$ and $CA_{DS=0.9}$/TEMPO-CNF films exhibited characteristic wavy patterns of thermal expansion against temperature. The expansion increased at the initial temperature stage, decreased to negative values at the second temperature stage, and then increased again at the third temperature stage. The thermal expansion ranges decreased as the TEMPO-CNF content increased.

The characteristic wavy patterns of thermal expansion of the CA-containing films remained unchanged after cooling, even after repeated heating or drying. Therefore, the results in Fig. 8 were not influenced by any moisture present in the films. Because $CA_{DS=0.9}$ contains both hydrophilic hydroxy groups with hydrogen bond-formable properties and hydrophobic acetyl groups with hydrophobic interaction-formable properties, the degrees of hydrogen bond and/or hydrophobic bond formation change reversibly in the films, depending on the temperature, in contrast to the 100 % TEMPO-CNF films. However, these hypotheses require further verification.

4. Conclusions

In the present study, we prepared transparent $CA_{DS=0.9}$/TEMPO-CNF composite films with TEMPO-CNF contents of up to 16 % by mixing aqueous CA solutions and aqueous TEMPO-CNF dispersions (i.e., entirely aqueous systems) in various mass ratios, and casting and drying the mixtures. The CA/TEMPO-CNF composite films produced disordered XRD patterns, irrespective of the TEMPO-CNF content. The tensile strength and Young's modulus of each film increased as the TEMPO-CNF content increased, and when the TEMPO-CNF content was 16 %, they reached over twice the values of a 100 % CA film. Therefore, the presence of crystalline TEMPO-CNFs in the $CA_{DS=0.9}$ base polymer clearly improved the tensile properties of the composite films. The film cross-sections revealed almost homogeneous and individual distribution of the TEMPO-CNF-COOH elements, and the films retained the nanofiber morphologies of the original composite films, as indicated by TEM. In contrast, the TEMPO-CNF-COONa elements aggregated slightly in the middle and bottom surface layers. The 100 % $CA_{DS=0.9}$ film exhibited characteristic wavy thermal expansion patterns from positive and negative expansion at 30–100 °C. The absolute expansion was reduced by the addition of crystalline TEMPO-CNFs, although the wavy patterns were retained.

Funding

This study was supported in part by the New Energy and Industrial Technology Development Organization (NEDO), Japan. GH thanks the China Scholarship Council (CSC) for financial support. KC is a recipient of a Japan Monbu-Kagakusho (MEXT) Fellowship for Foreign Ph.D. Students.

CRediT authorship contribution statement

Hongrun Chen: Writing – original draft, Visualization, Methodology, Formal analysis, Data curation. **Gaoyuan Hou:** Writing – review & editing, Methodology, Formal analysis, Data curation. **Korawit Chitbanyong:** Writing – review & editing, Validation, Methodology, Data curation. **Miyuki Takeuchi:** Writing – review & editing, Visualization, Methodology. **Izumi Shibata:** Writing – review & editing, Methodology, Formal analysis. **Akira Isogai:** Writing – review & editing, Supervision, Resources, Project administration, Investigation, Funding acquisition, Conceptualization.

Declaration of competing interest

The authors have no conflicts of interest to declares.

Data availability

Data will be made available on request.

Acknowledgments

We would like to thank Dr. Haruo Konno of Nippon Paper Ind. for kindly providing the TEMPO-CNF sample. We thank Edanz for editing a draft of this manuscript.

Appendix A. Supplementary data

Supplementary data to this article can be found online at https://doi.org/10.1016/j.reactfunctpolym.2024.106083.

References

[1] C.J. Malm, L.J. Tanghe, B.C. Laird, Preparation of cellulose acetate - action of sulfuric acid, Ind. Eng. Chem. 38 (1946) 77–82.

[2] H. Steinmeier, Cellulose Acetates: Properties and Applications, Macromol. Symp, Wiley, Heidelberg, 2004, p. 208. ISBN 3-527-31041-x.

[3] S. Fischer, et al., Properties and applications of cellulose acetate, Macromol. Symp. 262 (2008) 89–96.

[4] K. Okahashi, M. Takeuchi, Y. Zhou, Y. Ono, S. Fujisawa, T. Saito, A. Isogai, Nanocellulose-containing cellulose ether composites films prepared from aqueous mixtures by casting and crying method, Cellulose 28 (2021) 6373–6387, https://doi.org/10.1007/s10570-021-03897-5.

[5] T. Heinze, J. Schleller, New water soluble cellulose esters synthesized by an effective acylation procedure, Macromol. Chem. Phys. 201 (2000) 1214–1218, https://doi.org/10.1002/1521-3935(20000801)201:12.

[6] J. Pang, M. Wu, X. Liu, B. Wang, J. Yang, F. Xu, M. Ma, X. Zhang, Three-dimensional layered water-soluble cellulose acetate/polyacrylamide composites with ultrahigh ductility and stretchability, Sci. Rep. 7 (2017) 13233, https://doi.org/10.1038/s41598-017-13374-4.

[7] A.K. Mukherjee, R.K. Agarwal, H.K. Chaturvedi, B.D. Gupta, Water-soluble cellulose acetate and its application, Indian J. Text. Res. 6 (1981) 120–123.

[8] C.M. Buchanan, K.J. Edgar, A.K. Wilson, Preparation and characterization of cellulose monoacetates: the relationship between structure and water solubility, Macromolecules 24 (1991) 3060–3064, https://doi.org/10.1021/ma00011a005.

[9] S. Gomez-Bujedo, E. Fleury, M.R. Vignon, Preparation of cellouronic acids and partially acetylated cellouronic acids by TEMPO-NaClO oxidation of water-soluble cellulose acetate, Biomacromolecules 5 (2004) 565–571, https://doi.org/10.1021/bm034405y.

[10] A. Hummel, 3.2 Industrial processes, in: H. Steinmeier (Ed.), Cellulose Acetates: Properties and Applications 208, Macromol. Symp, Wiley, Heidelberg, 2004, pp. 61–79, https://doi.org/10.1002/masy.200450406.

[11] E. Samios, R.K. Dart, J.V. Dawkins, Preparation, characterization and biodegradation studies on cellulose acetates with varying degrees of substitution, Polymer 38 (1997) (1997) 3045–3054.

[12] C. Altaner, B. Saake, J. Puls, Mode of action of acetylesterases associated with endoglucanases towards water-soluble and -insoluble cellulose acetates, Cellulose 8 (2001) 259–265, https://doi.org/10.1023/A:1015164311521.

[13] J. Puls, S.A. Wilson, D. Hölter, Degradation of cellulose acetate-based materials: a review, J. Polym. Environ. 19 (2011) 152–165, https://doi.org/10.1007/s10924-010-0258-0.

[14] T.A. Wheatley, Water soluble cellulose acetate: a versatile polymer for film coating, Drug Dev. Ind. Pharm. 33 (2007) 281290, https://doi.org/10.1080/03639040600683469.

[15] A. Isogai, Emerging nanocellulose technologies: recent developments, Adv. Mater. 33 (2021) 2000630, https://doi.org/10.1002/adma.202000630.

[16] H. Fukuzumi, T. Saito, T. Iwata, Y. Kumamoto, A. Isogai, Transparent and high gas barrier films of cellulose nanofibers prepared by TEMPO-mediated oxidation, Biomacromolecules 10 (2009) 162–165, https://doi.org/10.1021/bm801065u.

[17] A. Isogai, T. Saito, H. Fukuzumi, TEMPO-oxidized cellulose nanofibers, Nanoscale 3 (2011) 71–85, https://doi.org/10.1039/c0nr00583e.

[18] I. Homma, H. Fukuzumi, T. Saito, A. Isogai, Effects of carboxyl-group counter-ions on biodegradation behaviors of TEMPO-oxidized cellulose fibers and nanofibril films, Cellulose 20 (2013) 2505–2515, https://doi.org/10.1007/s10570-013-0020-6.

[19] R. Endo, T. Saito, A. Isogai, TEMPO-oxidized cellulose nanofibril/poly(vinyl alcohol) composite drawn fibers, Polymer 54 (2013) 935–941, https://doi.org/10.1016/j.polymer.2012.12.035.

[20] T. Kurihara, A. Isogai, Properties of poly(acrylamide)/TEMPO-oxidized cellulose nanofibril composite films, Cellulose 21 (2014) 291–299, https://doi.org/10.1007/s10570-013-0124-z.

[21] Z. Shi, H. Xu, Q. Yang, C. Xiong, M. Zhao, K. Kobayashi, T. Saito, A. Isogai, Carboxylated nanocellulose/poly(ethylene oxide) composite films as solid–solid phase-change materials for thermal energy storage, Carbohydr. Polym. 225 (2019) 115215, https://doi.org/10.1016/j.carbpol.2019.115215.

[22] S. Ukita, H. Taniguchi, S. Shimamoto, T. Nakamura, Cellulose acetate with a low degree of substitution, US Pat. 10703825B2, 2020.

[23] T. Takeuchi, E. Miyauchi, T. Kanaya, et al., Acetate differentially regulates IgA reactivity to commensal bacteria, Nature 595 (2021) 560–564, https://doi.org/10.1038/s41586-021-03727-5.

[24] S. Fujisawa, Y. Okita, H. Fukuzumi, T. Saito, A. Isogai, Preparation and characterization of TEMPO-oxidized cellulose nanofibril films with free carboxyl groups, Carbohydr. Polym. 84 (2011) 579–583, https://doi.org/10.1016/j.carbpol.2010.12.029.

[25] K. Chitbanyong, G. Hou, M. Takeuchi, I. Shibata, A. Isogai, β-(1→4)-Polyglucuronic acids with C2/C3-ketones prepared from regenerated cellulose by catalytic oxidation using solid $NaOCl{\cdot}5H_2O$, Carbohydr. Polym. 343 (2024) 122458, https://doi.org/10.1016/j.carbpol.2024.122458.

[26] W. Mäntele, E. Deniz, UV–VIS absorption spectroscopy: Lambert-beer reloaded, Spectrochim. Acta A Mol. Biomol. Spectrosc. 173 (2017) 965–968, https://doi.org/10.1016/j.saa.2016.09.037.

[27] Standard Test Method for Haze and Luminous Transmittance of Transparent Plastics, ASTM D1003-21, 2021.

[28] Y. Zhou, Y. Ono, M. Takeuchi, A. Isogai, Changes to the contour length, molecular chain length, and solid-state structures of nanocellulose resulting from sonication in water, Biomacromolecules 21 (2020) 2346–2355, https://doi.org/10.1021/acs.biomac.0c00281.

[29] T. Miyamoto, Y. Sato, T. Shibata, ^{13}C-NMR spectral studies on the distribution of substituents in water-soluble cellulose acetate, J. Polym. Sci. Polym. Chem. Ed. 23 (1985) 1373–1381, https://doi.org/10.1002/pol.1985.170230511.

[30] T. Heinze, T. Liebert, 4.2. Chemical characteristics of cellulose acetate, in: H. Steinmeier (Ed.), Cellulose Acetates: Properties and Applications 208, Macromol. Symp, Wiley, Heidelberg, 2004, pp. 167–237, https://doi.org/10.1002/masy.200450408.

[31] M. Nogi, S. Iwamoto, A.N. Nakagaito, H. Yano, Optically transparent nanofiber paper, Adv. Mater. 21 (2009) 1595–1598, https://doi.org/10.1002/adma.200803174.

[32] H. Yagyu, T. Saito, A. Isogai, H. Koga, M. Nogi, Chemical modification of cellulose nanofibers for the production of highly thermal resistant and optically transparent nanopaper for paper devices, ACS Appl. Mater. Interfaces 7 (2015) 22012–22017, https://doi.org/10.1021/acsami.5b06915.

[33] M. Nogi, C. Kim, T. Sugahara, T. Inui, T. Takahashi, K. Suganuma, High thermal stability of optical transparency in cellulose nanofiber paper, Appl. Phys. Lett. 102 (2013) 181911, https://doi.org/10.1063/1.4804361.

[34] Y. Nishiyama, Structure and properties of the cellulose microfibril, J. Wood Sci. 55 (2009) 241–249, https://doi.org/10.1007/s10086-009-1029-1.

[35] D.R. Paul, L.M. Robeson, Polymer nanotechnology: nanocomposites, Polymer 49 (2008) 3187–3204, https://doi.org/10.1016/j.polymer.2008.04.017.